energy&fuels

Article

pubs.acs.org/EF

Some Aspects of the Mechanism of Formation of Smoke from the Combustion of Wood

F. A. Atiku,[†] A. R. Lea-Langton,[‡] K. D. Bartle,[†] J. M. Jones,[†] A. Williams,*[,†] I. Burns,[§] and G. Humphries[§]

[†]School of Chemical and Process Engineering, University of Leeds, Leeds LS2 9JT, U.K.

[‡]School of Mechanical, Aerospace and Civil Engineering, Manchester University, Manchester M13 9PL, U.K.

[§]Chemical and Process Engineering, University of Strathclyde, Glasgow G1 1XQ, U.K.

Supporting Information

ABSTRACT: This paper is concerned with an investigation of the formation of soot from the combustion of some of the primary pyrolysis products formed during pine wood combustion. Comparisons are made between the combustion products of model compounds, furfural for cellulose and eugenol and anisole to represent lignin (and *n*-decane for comparison) with the smoke emissions from the previously studied combustion of pine wood. These compounds were burned in a diffusion flame burner, and the appearance and composition of the resulting particulate and the adsorbed polynuclear aromatic hydrocarbon (PAH) precursors were studied by transmission electron microscopy (TEM), mass spectrometry and pyrolysis gas chromatography mass spectrometry (Py-GC-MS). The reactions leading to soot formation were modeled. It was concluded that wood soot formation proceeded via pyrolytic breakdown followed by a mechanism based on HACA (H-abstraction−C_2H_2-addition) reactions with the participation of cyclopentadienyl intermediates, while eugenol soot originated predominantly through the CPDyl route. The formation of furfural soot is mainly via HACA.

1. INTRODUCTION

The combustion of wood is widely used as a major source of heat and power covering a range of thermal capacities from domestic appliances to large scale generation plants, the attraction being in that they use a renewable energy source which is approximately carbon dioxide neutral.[1] The utilization of all fuels including biomass is subject to increasingly severe environmental legislation in terms of toxic gaseous pollutants and particulates.[2] In particular the formation of smoke arising mainly from incomplete combustion in small scale domestic units presents major environmental problems both from being a health hazard[3] and as a major contributor to climate change.[4,5] The emission of carbonaceous particles is an important factor in climate models.[4] Two major light-absorbing components of these particles are recognized:[5] black carbon (BC) which absorbs across the solar spectrum and light-absorbing organic carbon (OC, or BrC, brown carbon, coated on the BC particles) which absorbs at short wavelengths. Information about the chemical nature and origin of these species is required if their absorptive and hence warming effects are to be understood.

The general mechanism of wood combustion and the concomitant generation of environmentally unfriendly emissions have been extensively studied for a number of years.[2,6,7] The cellulose and lignin components can largely be considered to react separately.[8] The cellulose decomposes readily at high temperatures to CO and H_2 together with some small organic molecules; the lignin element decomposes to give much more complex mainly phenolic aromatic products. We have proposed that the cellulose products can form smoke largely via the H-abstraction−C_2H_2-addition, termed the HACA[9] route, and the lignin decomposition products form smoke via an aromatic species mechanism.[10,11]

Both hard and soft woods give similar devolatilization products although the distribution of the products is different, this resulting from the differences in the lignin content. GC-MS analysis shows that the principal initial volatile decomposition products of pine—a soft wood—include carbohydrate-derived material such as levoglucosan and furans,[11,12] and at higher temperatures the guaiacols and syringols from the lignin. In flames these decompose and form smaller but more thermally stable cyclic oxygenates and polycyclic aromatic compounds become significant species.[6,11,13] Some of the dominant primary products are furfuryl alcohol, furfural, and levoglucosan from the cellulose, and eugenol, isoeugenol, vanillin, and guaiacols from the lignin. Overall the products can be estimated using a computer model such as FG-Biomass.[2,14]

Furfural (furan-2-carbaldehyde) has been taken to be a typical product associated with cellulose pyrolysis and eugenol (2-methoxy-4-allylphenol or 4-allylguaiacol) to be associated with lignin. The structures and terminology of the major species used in this paper are given in Table 1 in the Supporting Information. Previous studies have been made by us of the formation of smoke and PAH arising from the combustion of these compounds in diffusion flames using aerosol time-of-flight mass spectrometry (ATOFMS).[13] There is considerable interest in the significance of these products from the thermal decomposition of biomass not only because of the importance

Received: October 11, 2016
Revised: January 16, 2017
Published: January 16, 2017

DOI: 10.1021/acs.energyfuels.6b02639
Energy Fuels 2017, 31, 1935−1944

Table 1. Combustion Properties of the Fuels

fuel	Bp, °C	smoke point, mm	mass burning rate, mg/s	emission factor, mg soot/g fuel	relative deposition rate of soot, mg/(g fuel s)	C/H ratio
n-decane	174.1	27.0	5.4	0.18	0.04	0.45
furfural	161.7	16.0	4.8	27.0	0.02	1.25
anisole	154	11.0	4.7	17.1	0.08	0.88
eugenol	254	6.5	1.4	132.2	0.11	0.83
furfural/eugenol 50/50 wt %		12.0	3.1	52.2	not determined	1.0

of these compounds in combustion but for the synthesis of chemical products; recent detailed studies have been made for cellulose,[15] lignin,[16] furfural,[17] anisole,[18] and eugenol.[19] In the present study we have extended our earlier work[13,20,21] on the processes leading to the formation of particulate soot.

2. EXPERIMENTAL SECTION

The liquid model fuels furfural, anisole, and eugenol were burned as diffusion flames as well as *n*-decane which was included for comparison purposes as a typical hydrocarbon fuel. All fuels were supplied by Sigma-Aldrich, UK and were >99% pure. The practical difficulty with studying combustion of high molecular weight fuels such as these is that it is not possible to vaporize them to produce gaseous premixed or diffusion flames because they decompose. The use of a wick burner overcomes this problem and this has been previously used by us,[13,21] but there are problems with repeatability and the inability to produce precision cylindrically symmetrical flames. We have attempted to reduce these errors by using a constant wick size and a uniform surrounding air flow; for all experiments a wick diameter of 2 mm and height of 7 mm was used. However, other refinements are possible and this issue has been addressed by others.[22] The other option of burning these fuels on a porous ceramic substrate such as a sphere is also not possible because of carbon deposition on the ceramic surface.[23]

The flames were photographed either directly or through a 430 nm optical filter to give an image of the CH* chemiluminescence,[24] which is a marker of the main reaction zone. The mass burning rates for the liquid fuels were determined gravimetrically, that is, by measuring the mass loss over a known time interval. Measurements of the smoke point were made using the ASTM D1322 Smoke Point Test.

Samples of pine wood were burned in an analogous way using small vertical strips of wood burned as a diffusion flame. The composition of the pine on a dry basis was: C 47.5 wt %, H 6.1 wt %, N 0.2 wt %, volatile matter 86.2 wt %, and ash 0.4 wt %. The pine consisted of 50% cellulose, 20% lignin, and 6% moisture, the remainder being hemicellulose and ash.

Laser-induced incandescence (LII) measurements[25,26] were made using a pulsed Nd:YAG laser (Surelite Continuum) emitting at 1064 nm. Excitation was undertaken using a beam with 1 mm diameter and a top-hat spatial profile. The time-resolved LII signal was imaged onto a 1 mm diameter pinhole and detected using a photomultiplier tube (Hamamatsu R636-10) with a narrow band-pass filter centered at 450 nm. Averages of 64 signal decays were recorded. Measurements were made 10 mm above the top of the wick at a range of radial locations. These measurements were performed in flames of *n*-decane, furfural, anisole, and eugenol. Soot volume fractions were quantified by comparing peak signal levels to measurements when the wick burner was replaced with a laminar flat flame of premixed ethene and air, in which the soot volume fraction was determined by extinction measurements. Temporal decay profiles allowed particle size to be estimated.[25,26]

The formation of soot was determined: (i) by measuring the total soot emitted by collecting and filtering all the combustion products; (ii) by deposition on a cold glass slide as previously described;[27] and (iii) by withdrawing soot samples directly from within the flame zone captured on electron microscope grids as used by Saffaripour et al.[28] and Kholghy et al.[29] using a 0.2s residence time. The soot samples were analyzed directly by Py-GC-MS as previously described;[10] 2 mg samples were heated to 400 °C with a ramp rate of 20 °C/ms and with a hold time of 20 s. Particle sizes of soot from the flame were determined by a Fast Particle Analyzer DMS 500 (Cambustion Ltd.) with samples being removed 5 cm above the flame tip by a sampling probe.

Computations of the opposed diffusion flames were made using the OPPDIF program contained within ANSYS Chemkin-Pro[30] computer code suite and the POLIMI 2012 chemical mechanism,[31] although with some additional reactions to the mechanism which are described later. The opposed-flow diffusion flame simulator, OPPDIF, is a steady-state solution which is computed for a diffusion flame between two opposing gas flows, one for the fuel and the other for the oxidant (air). The opposed two-dimensional flow is reduced mathematically to a one dimension simplification in which the fluid properties are functions of the distance only. The one-dimensional model then predicts the species, temperature, and velocity profiles in the flow between the sources. The model requires input data for reaction kinetics for all the reactions, along with thermodynamic data for all the species in a Chemkin format with 14 polynomial fitting coefficients to enable specific heats and enthalpies to be calculated up to the maximum flame temperature. Transport data are also required in a format to enable diffusion coefficients and thermal conductivities to be calculated for all species over the temperature range.

3. RESULTS AND DISCUSSION

3.1. Flame Studies. The model fuels studied were furfural, anisole, eugenol, and a conventional hydrocarbon fuel, namely *n*-decane. Their mass burning rates were determined to an accuracy of ±5% and are given in Table 1 together with the values for the smoke point index, smoke emission factors (mass smoke produced/mass fuel burned, the errors being ±10%), deposition rates, and the fuel C/H ratios. The values of the smoke points are given in descending order and include results for a 50/50 mixture of furfural and eugenol. It is clear that eugenol has the highest smoking tendency (lowest smoke point) and the highest emission factor. The deposition rates are a function of the soot volume fraction, the particle density and the thermophoretic drift, which in turn is a function of the temperature gradient at the boundary layer.[28] Because of the differences in burning rates they are presented here in relative terms of mass soot/mass fuel burned/s for the same surface area in all experiments. The errors here are ±20%. The results follow the smoke point data, but the C/H ratios and the emission factors do not; in both cases furfural behaves in an anomalous way, presumably because of its oxygen content.

Direct photographs were taken of all the flames and two typical flames, namely from furfural and anisole, are shown in Figure 1a and b. Eugenol produced a flame similar to anisole, but it had a lower mass burning rate and a smaller flame and clearly produced more soot especially concentrated along the central axis of the burned gases. The direct flame photographs were scanned by a densitometer and profiles of the visible soot emission obtained. By this method the order of soot propensity at 2 cm above the wick for all the flames is *n*-decane < furfural = anisole < eugenol.

DOI: 10.1021/acs.energyfuels.6b02639
Energy Fuels 2017, 31, 1935−1944

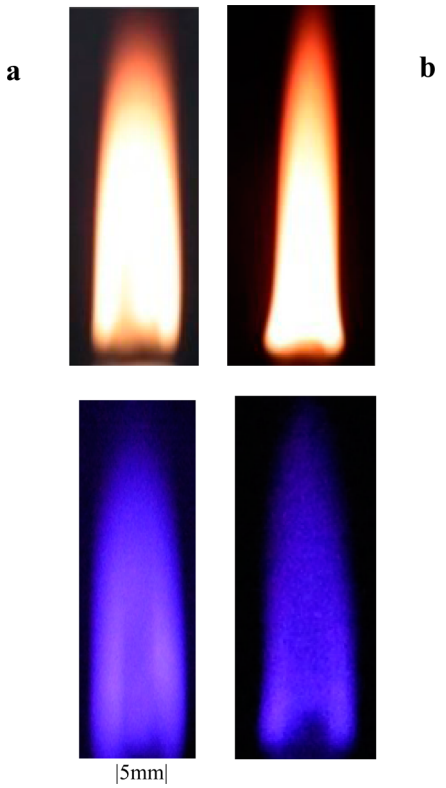

Figure 1. (top) Direct photographs of (a) furfural and (b) anisole flames on a wick burner. (bottom) CH* emission of the same flames through a 430 nm filter.

The soot forming zones in the flames were examined using LII. The soot volume fractions and primary particle sizes determined are shown in Figure 2 for the *n*-decane, anisole, furfural and eugenol flames. Each of the flames exhibits a peak soot volume fraction at a specific distance from the centerline, and these are consistent with the flame photographs. The anisole and furfural flames have a peak soot volume fraction of about 1 ppm, although the width of the soot-containing region varies between these flames. The *n*-decane flame has a peak soot volume fraction that is about three times lower than that of the other flames. The data obtained for the eugenol flames are also given in Figure 2, but there were measurement problems because of flame flickering resulting from soot deposition on the wick. High and intermittent LII signals were obtained when the thin soot front of the eugenol flame drifted into the measurement volume. The intermittently high soot volume fraction in the beam path for the eugenol flame also gave rise to an audible photoacoustic signal, consistent with a much higher soot volume fraction than in the other flames.

The results given in Figure 2 for the soot particle sizes in the measurement volume show that all the smallest particles are in the *n*-decane flame (about 35 nm diameter) and that there is little change in the size across the flame radius. Both furfural and anisole flames show similar behavior with particles with diameters of about 35 and 60 nm, respectively. The eugenol flame behaves slightly differently; it has larger particles (60 nm) in the core decreasing to about 40 nm on the outside which is believed to result from the fact that the core of the flame had visibly higher soot levels

3.2. Postflame Studies of Soot Formation. The diameters of the soot particles, D_p, emitted from the *n*-decane, furfural, and anisole flames which were sampled by a probe at 5

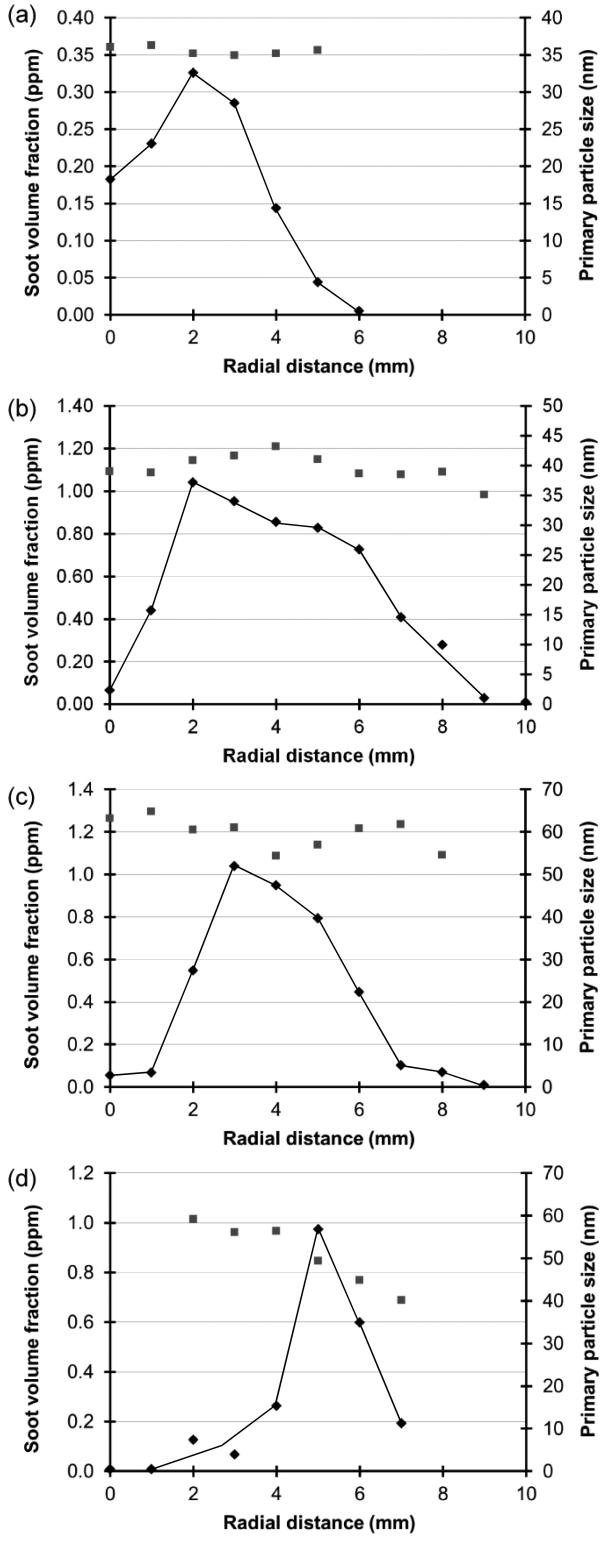

Figure 2. Soot volume fraction (diamonds) and primary particle size (squares) measured by LII as a function of radial position in the wick flames: (a) *n*-decane; (b) anisole; (c) furfural; (d) eugenol.

cm above the flame tip were determined using the DMS instrument. The results for all the flames followed a similar pattern and this is demonstrated for the anisole flame shown in Figure 3. It shows an initial group of particles of about 20 nm diameter, a second smaller group at about 60 nm diameter and a third major group with sizes up to 400 nm but peaking at 200

DOI: 10.1021/acs.energyfuels.6b02639
Energy Fuels 2017, 31, 1935−1944

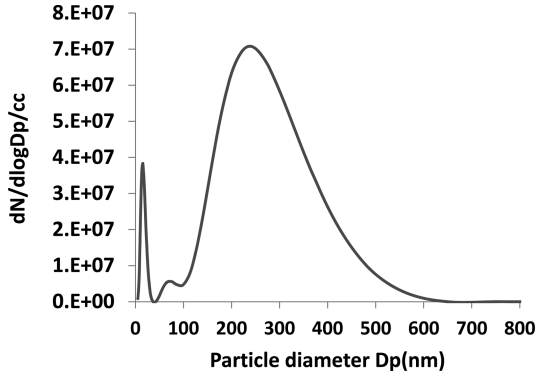

Figure 3. Graph of relative particle numbers (dN/dlog D_p/cc) against particle diameter D_p (nm) at 5 cm above the flame tip for anisole.

nm. The first two are consistent with the LII measurements while the latter group consists of chains of particles of the type commonly seen in combustion smoke and which were observed here by electron microscopy (but not shown here). It is interesting that the main peak starts from about 50 nm diameter. Particles of this size are identified in all the previous LII measurements and in the TEM photographs shown in Figure 4. However, in the anisole flame there is rapid agglomeration of the 50 nm particles to form chain structures and eventually fluffy soot. The DMS of the eugenol soot has previously been shown to be slightly different[32] with extensive agglomeration of particle with sizes above 1000 nm and this is consistent with the early stages of the formation of the cotton-like structures described earlier.

Soot samples were obtained by deposition on a plate placed 5 cm above the flame using the method previously used before for ethene flames.[27] It was clear that there were two significantly different classes of deposits. The furfural diffusion flame gave a dense soot deposit similar to that found previously from ethene flames.[27] However, anisole and especially the eugenol flames, produced greater yields of a cotton-like soot aggregates typical of soot from benzene pyrolysis or flames.[33] Samples were examined by TEM and the first group was found to consist of spherical samples with about 20−40 nm diameter. The second group which overall was cotton-like actually consisted of clusters of chains of spherical particles with diameters of individual soot particles of about 40−60 nm. These clusters are fragile and are easily fragmented.

Soot particles were withdrawn by the electron microscope grid sampling probe from inside the flame as well as from above the flame. The samples were taken 10 mm above the combustion zone (because of the geometrical complexity of these flames) and examined by transmission electron microscopy (TEM). Here the particle diameters were about 10−15 nm in diameter for all the flames, increasing in size with reaction time to the exit particle size of 40−60 nm. Many of the particles are in the form of chains and thus had overall larger particle sizes, as shown in Figure 4a and b. Particles of soot from both in-flame and postflame samples of furfural and eugenol were examined by TEM microscopy. Examples of images of in-flame soot particles are shown in Figure 4a and b respectively. The furfural has discernible lamellae which form onion-like concentric rings while the eugenol soot has slightly more disordered regions of lamellae and slightly larger constituent units. Measurements of lattice spacing show that the difference is small: furfural 0.37 ± 0.05 and eugenol 0.45 ± 0.05. Postflame, the furfural and eugenol samples look very similar to both ordered regions and disordered regions in each set.

We have previously examined postflame samples of *n*-decane and the pine wood soot; *n*-decane soot is similar to furfural soot but more ordered, while the wood soot is largely amorphous with only a few pockets of graphitic structure.

Soot samples from pine wood and eugenol which were deposited on a cooled surface were analyzed by Py-GC-MS and the results are shown in Figure 5a and b, respectively. These results give an insight into the species involved in the formation of the soot in addition to condensed PAH aerosol particles, both of which have environmental implications.

The results may be interpreted as follows. In the case of pine-combustion generated soot the results are similar to those previously published,[10] but in that instance the soot was pyrolyzed at a higher temperature of 1000 °C and consequently some secondary pyrolysis products were also released. In this case the products deposited on the cooled surface showed the presence of the more stable cellulose decomposition products as well as those from the decomposition of lignin. The origin of pinewood soot precursors has been sought[10,11] in the reactions of terpenes and from the phenolic constituents of lignin. Under the conditions used here, we found that the PAH in the pine wood particulate contained mainly 2−4 rings (see Figure 5a); single-ring aromatics, and higher PAH were also generated. The potential importance of the CPDyl mechanism in wood

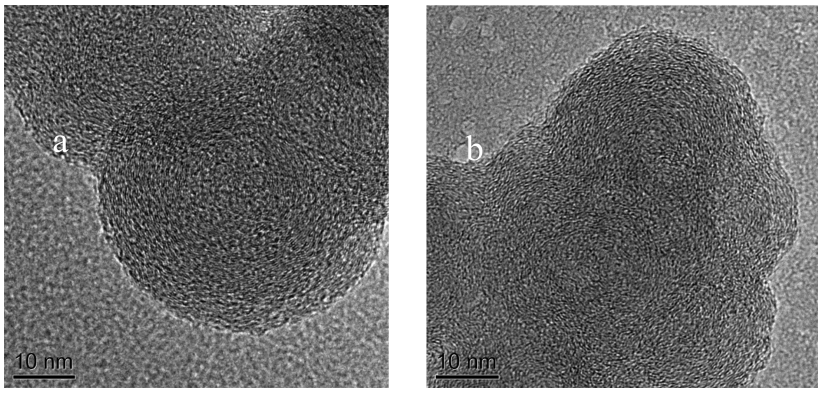

Figure 4. TEM images of soot particles deposited on an electron microscope grid sampled just after the reaction zone flame for (a) furfural and (b) eugenol, both high resolution (scale marked 10 nm).

DOI: 10.1021/acs.energyfuels.6b02639
Energy Fuels 2017, 31, 1935−1944

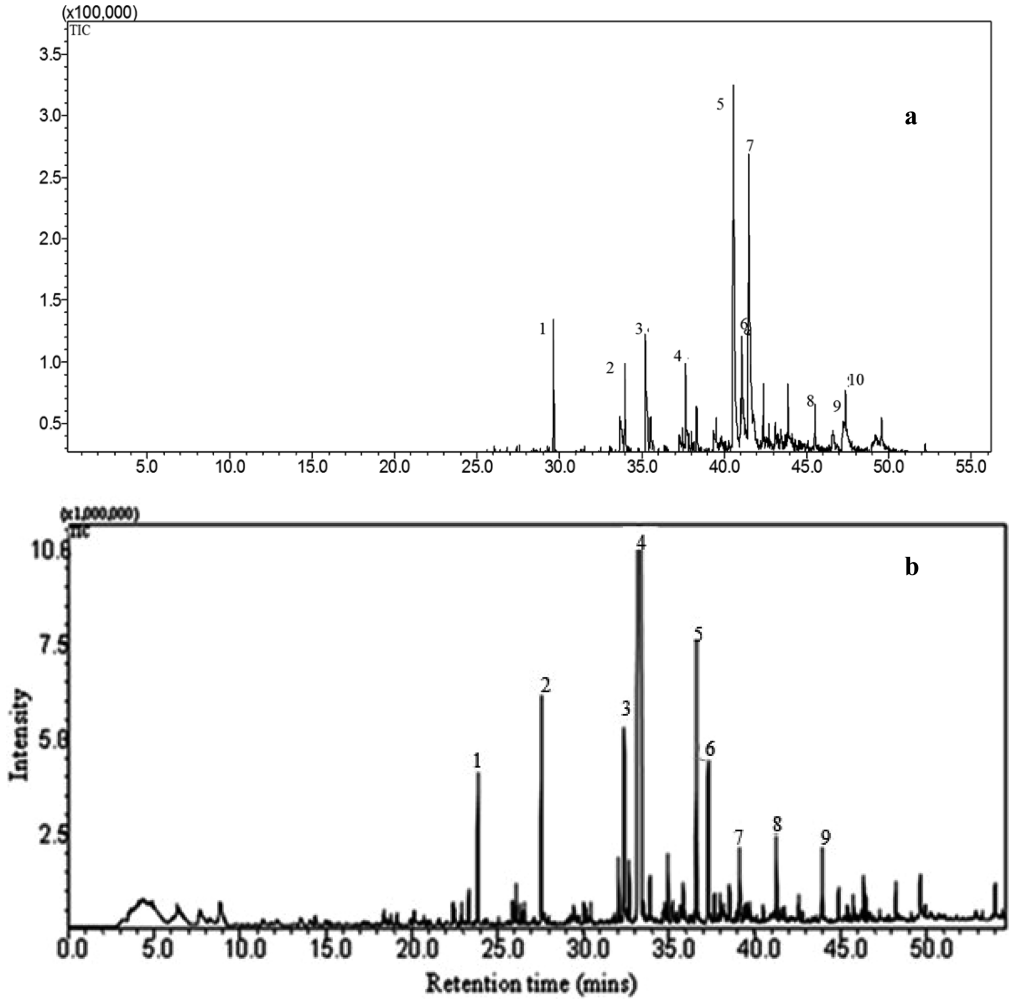

Figure 5. GC-MS plot (ion count against time) of adsorbed hydrocarbons pyrolyzed at 400 °C. (a) Pine wood flame soot: selected peak identifications 1, furan; 3, phenanthrene; 4, 4*H*-cyclopenta[*def*]phenanthrene; 5, fluoranthene; 6, acephenanthrylene; 7, pyrene; 8, l,2-(octadecyloxy)ethanol; 9, benzo[*ghi*]fluoranthene; 10, 3,4-di-*n*-butoxy-3 cyclobutene-1,2 dione. (b) Eugenol flame soot: 1, phenol; 2, guaiacol; 3, naphthalene; 4, 2-methoxy-4-methylphenol; 5, 4,7-dimethyl-3(2*H*)-benzofuranone; 6, eugenol; 7, isoeugenol; 8, phenanthrene. Other peaks are mainly complex phenols (phenanthroid) and some traces of phenalenes and pyrenes.

combustion seems clear in providing a starting point for the formation of PAH by the HACA route.[9] Simplified routes to soot from both aliphatic and aromatic fuels are shown in Figure 6a and b, respectively.

The HACA route is operative for both mechanisms, but CPDyl also plays a part for aromatics since monocyclic aromatics such as anisole, but also more complex phenols such as eugenol, give rise to a phenoxy radical which by the loss of CO forms CPDyl. The latter gives rise to indene and naphthalene, and from these hydrocarbons are derived a number of PAH leading to soot both by HACA[9] and by further reaction with CPDyl. This, like eugenol, produces aromatic like soot deposits and forms agglomerates. A major aromatic product from eugenol, the model for the structure of lignin during pyrolysis at the same temperature,[19] is also naphthalene, which is characteristic of the CPDyl mechanism for soot formation. After early growth from small PAH, the soot precursors grow further in four different general ways (Figure 6b).

The behavior of eugenol is of particular interest. The desorbed GC-MS results are shown in Figure 5b. It is clear that in these flames there are a considerable number of unreacted or partially reacted phenolic species which might participate in the soot forming processes. Of special interest is 2-methoxy-4-methylphenol (4-methylguaiacol), also identified in the products of bio-oil[34] from pyrolysis at a much lower temperature than that of the wick burner flame, thus suggesting early loss of the allyl group of eugenol. These phenols are expected to be precursors of CPDyl and importantly are components of the organic carbon (OC). Their composition depends very much on their thermal history but is in keeping with primary and secondary pyrolysis processes.[8] The presence of naphthalene in the eugenol soot (Figure 5 b) is consistent with a CPDyl mechanism, while the identification of higher MW PAH such as phenanthrene is indicative of a HACA route.

ATOFMS spectra of eugenol soot from a wick burner[13] are also consistent with a number of PAH formed by growth from naphthalene (MW 128 Da) through phenanthrene (178). A triad of peaks at 252, 276, and 300 Da is also prominent. The ATOFMS spectra also shows a series of peaks at $m/z > 250$ separated by 12 Da indicative of methyl addition to yield five-membered rings[35] and hence curvature in the growing soot.

3.3. Flame Computations—Mechanism of Smoke Formation. The reactions leading to the formation of soot

DOI: 10.1021/acs.energyfuels.6b02639
Energy Fuels 2017, 31, 1935−1944

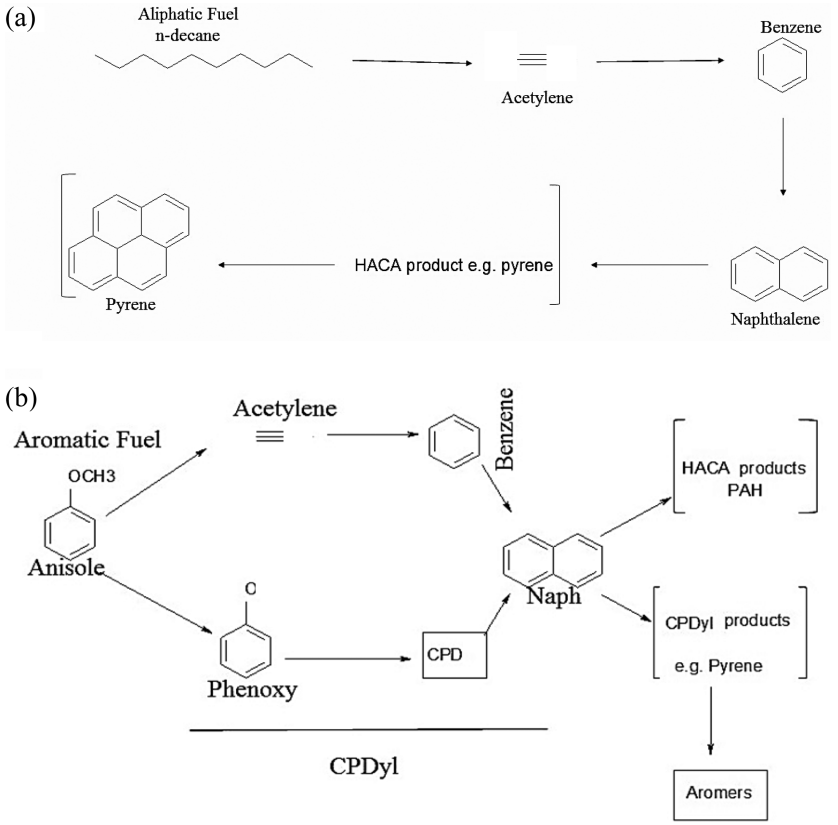

Figure 6. Routes to soot formation from (a) *n*-decane and (b) an aromatic fuel such as anisole.

was simulated using an opposed diffusion flame computation of the combustion of evaporated furfural, anisole or eugenol reacting with air, with both the air and the evaporated fuel stream preheated to 500 K. Computations were undertaken using the ANSYS Chemkin OPPDIF code[30] and the POLIMI 1201 combustion model.[31] This reaction mechanism employed pyrolysis and oxidation reactions occurring concurrently and involving up to 200 species and several thousand reactions. The model also calculates the concentrations of the species leading to the inception of soot. The growth of aromatics was followed from benzene to naphthalene ($C_{10}H_8$), to phenanthrene/anthracene ($C_{14}H_{10}$) and to pyrene/isomers ($C_{16}H_{10}$). The dimerization of pyrene is often associated with soot inception but in the present reaction mechanism growth is assumed using lumping reactions leading to the formation of BIN 1A ($C_{20}H_{16}$) and BIN 1B ($C_{20}H_{10}$); these species are used here as an indication of the onset of soot. The formation of some 5-carbon ring species is also included, namely indene (C_9H_8) and fluorene ($C_{13}H_{10}$). The mechanism also contains a reaction scheme for pyrolysis and oxidation of anisole and was used without change since it is consistent with recent published work.[18]

Models for the combustion of both *n*-decane and anisole are contained within the POLIMI 1201 program and it also contains the soot forming routes HACA and CPDyl. This mechanism has been validated and details are given in the references within ref 31. There are no published models for the initial reactions of the parent fuels furfural and eugenol and simplified schemes for these initial steps of these species were added to the POLIMI 1201 model. The basic combustion and soot forming schemes are the same as for anisole.

In the case of furfural, a mechanism largely based on recent publications[17,36] was adopted. At lower pyrolysis temperatures it is assumed that furfural undergoes unimolecular decomposition to furan + CO: $C_4H_3O{-}CHO\ (+\ M) \rightarrow CO + C_4H_4O$. Sequential decomposition of furan leads to the production of HC≡CH, CH_2CO, $CH_3C{\equiv}CH$, CO, $HCCCH_2$, and H atoms. At the higher flame temperatures we have taken:

$$\{C_4H_3O\}{-}CHO = \{C_4H_3O\} + HCO \quad (1)$$

$$\{C_4H_3O\} = C_3H_3 + CO \quad (2)$$

$$\{C_4H_3O\}{-}CHO + OH = \{C_4H_3O\}{-}CO + H_2O \quad (3)$$

$$\{C_4H_3O\}{-}CO = \{C_4H_3O\} + CO \quad (4)$$

$$\{C_4H_3O\}{-}CHO + CH_3 = \{C_4H_3O\}{-}CO + CH_4 \quad (5)$$

The structures and nomenclature of the new species involved are given in Table S1. Details of the kinetics of the added reactions are given in Table S2 in the Supporting Information. The rates chosen are based on analogous reactions in the main reaction scheme. In the case of reaction 4 we have used a second set of reaction rate parameters (4B). The former is based on a seeming similarity with reaction 1, but it has been pointed out that it is a radical alpha scission similar to CH_3CO. Thus, for reaction 4B we have used kinetic parameters appropriate to the decomposition of CH_3CO.

The only information on the mechanism for eugenol pyrolysis is from studies at lower temperatures.[19] The initial step used for eugenol is given below

$$\text{2-methoxy-4-allylphenol} = \{(C_6H_3)(OH)(OCH_3\} + C_3H_5 \quad (6)$$

DOI: 10.1021/acs.energyfuels.6b02639
Energy Fuels 2017, 31, 1935−1944

Table 2. Maximum Concentrations for Selected Species from Computed Opposed Diffusion Flames (Mole Fraction)

fuel	C_2H_2 (10^{-2})	cyclo-C_5H_5 CPDyl (10^{-3})	cyclo-C_5H_6 CPD (10^{-4})	C_6H_5O phenoxy (10^{-5})	C_9H_8 indene (10^{-4})	$C_{10}H_8$, naphthalene (10^{-3})	$C_{16}H_{10}$ pyrene (10^{-4})	BIN 1A/BIN 1B (10^{-4})
n-decane	2.3	0.07	4.5	0.004	0.8	0.3	1.0	0.2/1.1
furfural: run 4	1.6	0.05	0.28	0.003	8.9	0.9	14.4	104/160
furfural: run 4B	1.6	0.05	43	0.004	4.1	29	22.0	27/55
anisole	1.0	0.58	25.5	10.8	3.5	5.6	28.0	35/104
eugenol: model 1	66	1.6	20.4	3.2	44.4	6.0	30.8	106/144
eugenol:model 2	1.6	3.6	43	0.005	3.9	30	21.5	28/56

That is, eug = eugenyl-1 + C_3H_5

$$\text{eugenyl-1} = \text{eugenyl-2} + \text{CO} \quad (7)$$

$$\text{eugenyl-2} = \text{cyc-}C_5H_5 + CH_2O \quad (8)$$

where the C_3H_5, cyclic-C_5H_5, CH_2O, and CO would further react in the POLIMI 1201 mechanism scheme, but the remaining eugenyl radical presents many reaction route options. The derivation of eugenyl-2 from eugenyl-1 requires a phenoxy structure for loss of CO from eugenyl-1 and hence an isomerization of the initial eugenyl-1 structure to place the unpaired electron on the oxygen atom. The kinetic data used for eqs 6–8 are given in the Supporting Information.

In order to approximate the eugenol flame it was simplified and was considered to consist of equal amounts of anisole and C_3H_3 (termed Model 1). This is an approximation based on the premise that the allyl group breaks off the aromatic ring and is used in Model 1. It is contrary to the conclusions at lower temperatures where fission of the methoxy group occurs. Model 2 is based on reactions 6–8 and essentially the mechanism follows the formation of eugenyl-1 (C_7H_7O), then eugenyl-2 (C_6H_7O), and then to CPDyl, which gives a major route to soot precursors.

Computations were undertaken using OPPDIF for the combustion of *n*-decane, furfural using two sets of rate constants (4A and 4B), anisole, and two models for eugenol. The computed results give profiles of a large number of species through the flame zone culminating in an estimate of the point of soot formation inception represented by BIN 1A, BIN 1B, and the dimerization of pyrene. These give an indication of the soot inception region and the quantity of soot formed, but because of the way it is defined, it is therefore lower than the measured in-flame values given in Figure 2. Values for the maximum concentration of a number of these key species are given in Table 2. Two examples of the computed profiles are shown: furfural in Figure 7 using reaction 4 and for anisole in Figure 8. In these figures the fuel vapor approaches the reaction zone from the left-hand side and the air from the right-hand side, combustion takes place leading mainly to CO_2 and H_2O but with reactions leading to soot formation. The important soot-forming species shown in both figures are ethyne (acetylene), benzene, naphthalene and BIN 1A.

In the case of the furfural we obtained computed profiles for the two different rate parameter and the maximum concentrations obtained are shown in Table 2. The furfural run using the 4B rates gave an extremely wide reaction zone suggesting that the rate is too rapid. Bond distances were calculated using MOPAC 2012 and it was found that the molecule {C_4H_3O}—CO had a bond length of 0.141 nm while CH—CO had a bond length of 0.145 nm. This suggests that the bond dissociation for the former is greater and that the activation energy for reaction 4 is between the two sets of kinetic values used here. We have

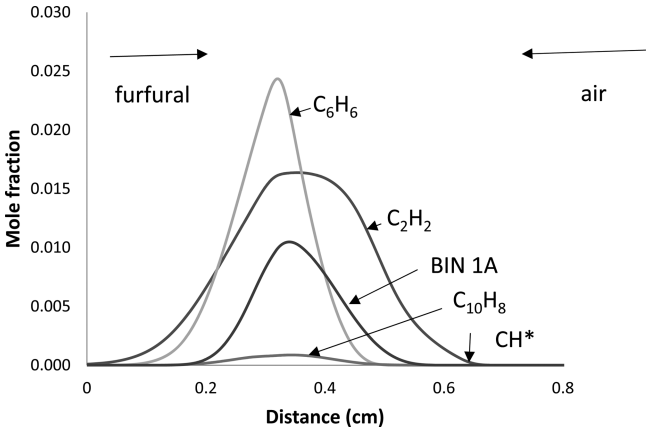

Figure 7. Computed opposed diffusion flames for furfural. The fuel flow is from the left-hand side and air from the right. The position of the maximum CH* chemiluminescent emission is indicated by a vertical arrow.

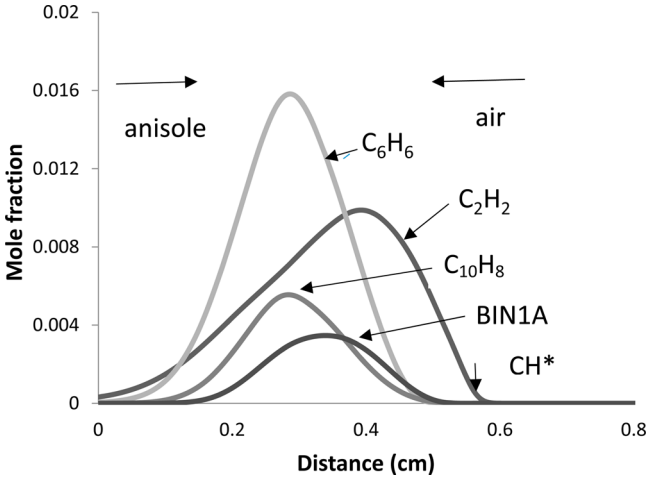

Figure 8. Computed opposed diffusion flames for anisole. The fuel flow is from the left-hand side and air from the right. The position of the maximum CH* chemiluminescent emission is indicated by a vertical line.

opted to show Figure 7 based on reaction 4, but clearly more information is required about this reaction, and preferably from a simpler reaction system.

n-Decane has also been studied and was found not to behave very differently from furfural, so this is representative of this class of products from cellulose: anisole is typical of the highly sooting polyphenol aromatic species produced by the pyrolysis of lignin.

The results obtained for both models for eugenol are given in Table 2 and listed as eugenol: Model 1 and eugenol: Model 2.

DOI: 10.1021/acs.energyfuels.6b02639
Energy Fuels 2017, 31, 1935–1944

Model 1 gave the higher soot output (BIN 1A, BIN 1B). Model 2 gave a soot precursor output (BIN 1A, BIN 1B) which is much lower than the Model 1 output, and indeed lower than that for furfural. The limitation with Model 2 is that it is entirely a pyrolysis model and does not include radical or atom attack on the parent molecule, nor include O−CH_3 fission because little is known about the reaction paths of the products. It was also suggested that we ran the model with an extra reaction, reaction 9 in Table S1, but this had no effect on the BIN 1A and BIN 1B output. Clearly additional reaction pathways are required as well as the examination of the kinetic parameters chosen.

These results show that in the flame zone *n*-decane and furfural which are cellulose products follow the HACA route. Eugenol is more aromatic and follows a different route and other species such as CPDyl play a prominent role. It also shows a correlation between the experimental emission factors in Table 1 and the values of BIN 1A, BIN 1B, and pyrene in Table 2. These have been used as indicators of the extent of soot formation.

The CH* chemiluminescent emission is considered to be the result of the C_2H + O reaction and an indicator of the position of the reaction zone, and the relative emission intensity was calculated on the assumption that it is proportional to their product. The positions of the maximum relative computed CH* chemiluminescence are shown in Figure 7a and b, and these are on the lean side of the combustion zones shown in Figure 1. The relative intensities of the CH* emission relative to *n*-decane are furfural 1.6 and anisole 0.5. These are consistent with the observations of the flames in Figure 1. The soot concentrations observed both visually or by LII are also consistent with the computed figures.

3.4. Soot Formation. The profiles of the higher PAH in soot resulting from wood combustion (such as pine) are consistent with the HACA route of PAH growth[9,35,37] to dense planar "protographite," molecules. However, pentagonal curved areas in this network (protofullerenes) can arise from five-membered rings;[38] these are bowl-shaped hydrocarbon structures which can lead to curvature of the sheet of carbon atoms and eventually to the curved or "onion-ring" morphology for the soot particle which can be seen by electron micrography, for example in Figure 2 for furfural and eugenol flame soots. These PAH structures can them stack and grow to soot particles[39−41] and chains and eventually graphitise further up in the flame.[22,29]

A route to (pine)wood soot involving "curved" protofullerenes is consistent with major contributions of a range of five-membered-ring PAH: 4*H*-cyclopenta[*def*]phenanthrene, acephenanthrylene, fluoranthene, and benzo[*ghi*]fluoranthrene; the concentrations of these exceeded those of identified six-membered ring compounds from which protographenes are derived. A number of studies have shown how five-membered ring PAH such as cyclopentapyrenes can isomerize to the bowl-shaped and highly reactive corannulene (C_{20}), MW 250, a species we have previously attributed in the direct introduction mass spectra of ethene soot.[37] Other bowl-shaped molecules, all subunits of fullerene, can be formed by dehydrocyclisation during pyrolysis of appropriate planar PAH containing five-membered rings, while the presence of hydrocarbons with a five-membered ring in the combustion of methane brought about a significant increase in sooting tendency.[38]

Models have been developed of the growth of these species into particle nuclei and beyond by growth through surface reactions and finally agglomeration. In order to follow these processes, various assumption are made and involve lumped species defined just by number of carbon atoms or molecular units with the aim of providing the mass and size distribution of total particulates. At the small molecular level it is possible to model the formation of the precursors (as in section 3.3), but the next step is more complex. Violi et al.[39] have used a detailed molecular model but only for the first stages leading to soot inception. In particular this uses the assumption that aromatic radicals add to the double bond of five-membered ring PAH. The typical size of the nucleus was first postulated by Wang et al.[42] to be that of circumcoronene, $C_{96}H_{24}$; this molecule contains 2% hydrogen, has dimensions 2 nm × 2 nm, and is consistent with the electron microscope images observed here (Figure 4), as well as by others.

Sirignano et al.[40] and Saggese et al.[41] have used growth models based on the following types of reaction:

$$\mathrm{Ri} + \mathrm{H} = \mathrm{Ri} + \mathrm{H_2} \quad (9)$$

$$\mathrm{Ri} + \mathrm{Ri} = \mathrm{Ri—Ri} \quad (10)$$

The products reach a size of about C_{96} but the structure may not be a uniform regular PAH. The growth picture is complicated by the fact that PAH species may just condense on the growing soot particle; this only acts as a condensation nucleus leading to a mixture of nearly pure soot, which agglomerates to form chains (see Figures 2−4) and droplets of mainly PAH.[5] This would explain the behavior of soot when deposited on cool surfaces as opposed to the behavior on hot surfaces. It follows that linking the soot forming mechanism quantitatively both to BC and to OC is complex and will be discussed elsewhere.

4. CONCLUSIONS

Representative species of wood pyrolysis products are furfural for cellulose and anisole and eugenol for lignin. Smoke emissions from their diffusion flames are initially the same and the initial soot particles grow to larger spherical particles. SEM measurements show that the initial particle sizes are approximately 30 nm and the particles agglomerate or aggregate to form chains. There is a significant difference between the final soot product from furfural and eugenol because of the aromatic nature and concentration of soot particles. This aromatic nature is not seen in biomass soot.

Furfural tends to follow the HACA route because of initial decomposition to suitable species that can follow this path. Eugenol undergoes side-chain cracking, followed by conventional phenol decomposition reactions, and also decomposition and reaction via cyclopentadiene.

Comparison has been made to pinewood soot which contains both organic carbon and black carbon. The decomposition products suggest an important PAH route is via cyclopentadiene, which is derived after cracking of lignin monomer fragments.

■ ASSOCIATED CONTENT

Supporting Information

The Supporting Information is available free of charge on the ACS Publications website at DOI: 10.1021/acs.energyfuels.6b02639.

Details of the structures in the reaction mechanism are given in Table S1 and the kinetic data in Table S2. The kinetic data are estimated values based on data for

DOI: 10.1021/acs.energyfuels.6b02639
Energy Fuels 2017, 31, 1935−1944

analogous reaction parameters given in ref 31. The furan terminology follows ref 36 (PDF)

AUTHOR INFORMATION

Corresponding Author

*E-mail: fueaw@leeds.ac.uk.

ORCID

A. Williams: 0000-0002-9841-3203

Notes

The authors declare no competing financial interest.

ACKNOWLEDGMENTS

We wish to acknowledge financial support from the EPSRC Supergen Bioenergy Hub (EP/J017302), F.A.A. wishes to acknowledge support from the TETFUND under the Kebbi State University for Science and Technology, Aliero, Nigeria. We also thank Professor A. S. Tomlin for the use of the DMS equipment, Mr. P. Mason for assistance with the optical experiments, and Dr. N. Hodran for assistance with the electron microscope measurements. We are indebted to the reviewers for some useful comments.

REFERENCES

(1) International Energy Agency. *Energy and Climate Change. World Energy Outlook Special Report*; IEA: Paris, 2015; www.iea.org.

(2) Williams, A.; Jones, J. M.; Ma, L.; Pourkashanian, M. Pollutants from the combustion of solid biomass fuels. *Prog. Energy Combust. Sci.* **2012**, *38*, 113−137.

(3) Bølling, A. K.; Pagels, J. K.; Yttri, E.; Barregard, L.; Sallsten, G. P.; Schwarze, P. E.; Boman, C. Health effects of residential wood smoke particles: the importance of combustion conditions and physicochemical particle properties. *Part. Fibre Toxicol.* **2009**, *6*, 29.

(4) Bond, T. C.; Doherty, S. J.; Fahey, D. W.; Forster, P.; Berntsen, T.; et al. Bounding the role of black carbon in the climate system. A scientific assessment. *J.Geophys. Res.: Atmos.* **2013**, *118*, 5380−5552.

(5) Dickau, M.; Olfert, J.; Stettler, M. E. J.; Boies, A.; Momenimovahed, A.; Thomson, K.; Smallwood, G.; Johnson, M. Methodology for quantifying the volatile mixing state of an aerosol. *Aerosol Sci. Technol.* **2016**, *50* (8), 759−772.

(6) Orasche, J.; Seidel, T.; Hartmann, H.; Schnelle-Kreis, J.; Chow, J. C.; Ruppert, H.; Zimmermann, R. Comparison of emissions from wood combustion. Part 1: Emission factors and characteristics from different small-scale residential heating appliances considering particulate matter and polycyclic aromatic hydrocarbon (PAH)-related toxicological potential of particle-bound organic species. *Energy Fuels* **2012**, *26* (10), 6695−6704.

(7) Eriksson, A. C.; Nordin, E. Z.; Nyström, R.; Pettersson, E.; Swietlicki, E.; Bergvall, C.; Westerholm, R.; Boman, C.; Pagels, J. H. Particulate PAH emissions from residential biomass combustion: Time-resolved analysis with aerosol mass spectrometry. *Environ. Sci. Technol.* **2014**, *48*, 7143−7150.

(8) Branca, C.; Di Blasi, C. A unified mechanism of the combustion reactions of lignocellulosic fuels. *Thermochim. Acta* **2013**, *565*, 58−64.

(9) Frenklach, M.; Wang, H. Detailed mechanism and modeling of soot particle formation. In *Soot Formation in Combustion: Mechanisms and Models*; Bockhorn, H., Ed.; Springer-Verlag: Berlin, 1994; pp165−192.

(10) Fitzpatrick, E. M.; Jones, J. M.; Pourkashanian, M.; Ross, A. B.; Williams, A.; Bartle, K. D. Mechanistic aspects of soot formation from the combustion of pine wood. *Energy Fuels* **2008**, *22* (6), 3771−3778.

(11) Fitzpatrick, E. M.; Bartle, K. D.; Kubacki, M. L.; Jones, J. M.; Pourkashanian, M.; Ross, A. B.; Williams, A.; Kubica, K. The mechanism of the formation of soot and other pollutants during the co-firing of coal and pine wood in a fixed bed combustor. *Fuel* **2009**, *88*, 2409−2417.

(12) Phillips, D.; Mitchell, E. J. S.; Lea-Langton, A. R.; Parmar, K. R.; Jones, J. M.; Williams, A. The use of conservation biomass feedstocks as potential bioenergy resources in the United Kingdom. *Bioresour. Technol.* **2016**, *212*, 271−279.

(13) Wilson, J. M.; Baeza-Romero, M. T.; Jones, J. M.; Pourkashanian, M.; Williams, A.; Lea-Langton, A. R.; Ross, A. B.; Bartle, K. D. Soot formation from the combustion of biomass pyrolysis products and a hydrocarbon fuel, n-decane: an ATOFMS study. *Energy Fuels* **2013**, *27* (3), 1668−1678.

(14) FG-Biomass. www.afrinc.com (accessed January 13, 2017).

(15) Wang, S.; Guo, X.; Liang, T.; Zhou, Y.; Luo, Z. Mechanism research on cellulose pyrolysis by Py-GC/MS and subsequent density functional theory studies. *Bioresour. Technol.* **2012**, *104*, 722−728.

(16) Zhang, T.; Li, X.; Qiao, X.; Zheng, M.; Guo, L.; Song, W.; Lin, W. Initial mechanisms for an overall behavior of lignin pyrolysis through large-scale ReaxFF molecular dynamics simulations. *Energy Fuels* **2016**, *30* (4), 3140−3150.

(17) Vasiliou, A. K.; Kim, J. H.; Ormond, T. K.; Piech, K. M.; Urness, K. N.; Scheer, A. M.; Robichaud, D. J.; Mukarakate, C.; Nimlos, M. R.; Daily, J. W.; Guan, Q.; Carstensen, H. H.; Ellison, G. B. Biomass pyrolysis: thermal decomposition mechanisms of furfural and benzaldehyde. *J. Chem. Phys.* **2013**, *139* (10), 104310.

(18) Nowakowska, M.; Herbinet, O.; Dufour, A.; Glaude, P.-A. Detailed kinetic study of anisole pyrolysis and oxidation to understand tar formation during biomass combustion and gasification. *Combust. Flame* **2014**, *161*, 1474−1488.

(19) Ledesma, E. B.; Campos, C.; Cranmer, D. J.; Foytik, B. L.; Ton, M. N.; Dixon, E. A.; Chirino, C.; Batamo, S.; Roy, P. Vapor-phase cracking of eugenol: distribution of tar products as functions of temperature and residence time. *Energy Fuels* **2013**, *27* (2), 868−878.

(20) Ross, A. B.; Junyapoon, S.; Jones, J. M.; Williams, A.; Bartle, K. D. A study of different soots using pyrolysis−GC−MS and comparison with solvent extractable material. *J. Anal. Appl. Pyrolysis* **2005**, *74*, 494−501.

(21) Baeza-Romero, M. T.; Wilson, J. M.; Fitzpatrick, E. M.; Jones, J. M.; Williams, A. In situ study of soot from the combustion of a biomass pyrolysis intermediate; eugenol and n-decane using aerosol time of flight mass spectrometry. *Energy Fuels* **2010**, *24* (1), 439−445.

(22) Botero, M. L.; Chen, D.; Gonzalez-Calera, S.; Jefferson, D.; Kraft, M. HRTEM evaluation of soot particles produced by the non-premixed combustion of liquid fuels. *Carbon* **2016**, *96*, 459−473.

(23) Bartle, K. D.; Fitzpatrick, E. M.; Jones, J. M.; Kubacki, M. L.; Plant, R.; Pourkashanian, M.; Ross, A. B.; Williams, A. The combustion of droplets of liquid fuels and biomass particles. *Fuel* **2011**, *90*, 1113−1119.

(24) Karnani, S.; Dunn-Rankin, D. Visualizing CH* chemiluminescence in sooting flames. *Combust. Flame* **2013**, *160*, 2275−2278.

(25) Schulz, C.; Kock, B. F.; Hofmann, M.; Michelsen, H.; Will, S.; Bougie, B.; Suntz, R.; Smallwood, G. Laser-induced incandescence: recent trends and current questions. *Appl. Phys. B: Lasers Opt.* **2006**, *83*, 333−354.

(26) Bladh, H.; Johnsson, J.; Olofsson, N.-E.; Bohlin, A.; Bengtsson, P.-E. Optical soot characterisation using two-color laser-induced incandescence (2C-LII) in the soot growth region of a premixed flat flame. *Proc. Combust. Inst.* **2011**, *33*, 641−648.

(27) Smedley, J. M.; Williams, A.; Mutshimwong, A. Soot deposition from ethylene/air flames and the role of aromatic intermediates. In *Soot Formation in Combustion: Mechanisms and Models*; Bockhorn, H., Ed.; Springer-Verlag: Berlin, 1994; pp 403−416.

(28) Saffaripour, M.; Veshkini, A.; Kholghy, M.; Thomson, M. J. Experimental investigation and detailed modeling of soot aggregate formation and size distribution in laminar coflow diffusion flames of Jet A-1, a synthetic kerosene, and n-decane. *Combust. Flame* **2014**, *161*, 848−863.

(29) Kholghy, M. R.; Veshkini, A.; Thomson, M. J. The core-shell internal nanostructure of soot - A criterion to model soot maturity. *Carbon* **2016**, *100*, 508−536.

(30) ANSYS Chemkin Pro. www.ansys.com (accessed January 13, 2017).

DOI: 10.1021/acs.energyfuels.6b02639
Energy Fuels 2017, 31, 1935−1944

(31) Ranzi, E.; Faravelli, T. *POLIMI 1201*; 2016; http://creckmodeling.chem.polimi.it (accessed January 13, 2017).
(32) Lea-Langton, A. R.; Baeza-Romero, M. T.; Boman, G. V.; Brooks, B.; Wilson, A. J. M.; Atika, F. A.; Bartle, K. D.; Jones, J. M.; Williams, A. A study of smoke formation from wood combustion. *Fuel Process. Technol.* **2015**, *137*, 327−332.
(33) Frusteri, L.; Cannilla, C.; Barbera, K.; Perathoner, S.; Centi, G.; Frusteri, F. Carbon growth evidences as a result of benzene pyrolysis. *Carbon* **2013**, *59*, 296−307.
(34) Stas, M.; Kubicka, D.; Chudoba, J.; Pospisil, M. Overview of analytical methods used for chemical characterization of pyrolysis bio-oil. *Energy Fuels* **2014**, *28*, 385−402.
(35) Shukla, B.; Koshi, M. Comparative study on the growth mechanisms of PAHs. *Combust. Flame* **2011**, *158*, 369−75.
(36) Tian, Z.; Yuan, T.; Fournet, R.; Glaude, P.-A.; Sirjean, B.; Battin-Leclerc, F.; Zhang, K.; Qi, F. An experimental and kinetic investigation of premixed furan/oxygen/argon flames. *Combust. Flame* **2011**, *158*, 756−773.
(37) Smedley, J. M.; Williams, A.; Bartle, K. D. A mechanism for the formation of soot particles and soot deposits. *Combust. Flame* **1992**, *91*, 71−82.
(38) McEnally, C. S.; Pfefferle, L. D. An experimental study in non-premixed flames of hydrocarbon growth processes that involve five-membered carbon rings. *Combust. Sci. Technol.* **1998**, *131*, 323−344.
(39) Violi, A.; Sarofim, A. F.; Voth, G. A. Kinetic Monte Carlo-molecular dynamics approach to model soot inception. *Combust. Sci. Technol.* **2004**, *176* (5−6), 991−1005.
(40) Sirignano, M.; Kent, J.; D'Anna, A. Modeling formation and oxidation of soot in nonpremixed flames. *Energy Fuels* **2013**, *27* (4), 2303−2315.
(41) Saggese, C.; Ferrario, S.; Camacho, J.; Cuoci, A.; Frassoldati, A.; Ranzi, E.; Wang, H.; Faravelli, T. Kinetic modeling of particle size distribution of soot in a premixed burner-stabilized stagnation ethylene flame. *Combust. Flame* **2015**, *162* (9), 3356−3369.
(42) Wang, T. S.; Matula, R. A.; Farmer, R. C. Combustion kinetics of soot formation from toluene. *Symp. Combust., [Proc.]* **1981**, *18*, 1149−1157.

DOI: 10.1021/acs.energyfuels.6b02639
Energy Fuels 2017, 31, 1935−1944